R E S E A R C H

Enhanced Arsenic Removal from Aqueous Solutions Via Magnesium Hydroxide Coated Iron Nanoparticles

Ibrahim Maamoun[1],* | **Omar Falyouna[2]** | **Islam Mir Shariful[3,4]** |
Ramadan Eljamal[5] | **Khaoula Bensaida[2]** | **Kazuya Tanaka[1]** |
Kohei Tokunaga[1,6] | **Osama Eljamal[2],***

[1]Advanced Science Research Center, Japan Atomic Energy Agency, Ibaraki, 319-1195, Japan
[2]Water and Environmental Engineering Laboratory, Interdisciplinary Graduate School of Engineering Sciences, Kyushu University, Fukuoka, 816-8580, Japan
[3]International Institute for Carbon-Neutral Energy Research (I2CNER), Kyushu University, Fukuoka, 819-0395, Japan
[4]Department of Oceanography, University of Dhaka, Dhaka-1000, Bangladesh
[5]Research Center for Negative Emission Technology, International Science Innovation Center, Kyushu University, Fukuoka, 819-0395, Japan
[6]Ningyo-toge Environmental Engineering Center, Japan Atomic Energy Agency, Tomata, Okayama, 708-0698, Japan

*Corresponding authors:
E-mail: maamoun.ibrahim@jaea.go.jp
(Ibrahim Maamoun)
osama-eljamal@kyudai.jp
(Osama Eljamal)
Tel.: +81-80-4278-8910
      +81-80-3900-8521

Web of Science Researcher ID:
Ibrahim Maamoun
(AAA-7992-2021)

A B S T R A C T

For several decades, arsenic (As) contamination of water was considered as an issue of great concern. In this study, magnesium hydroxide coated iron nanoparticles ($nFe^0@Mg(OH)_2$) were developed for enhancing arsenic removal from aqueous solutions. Several parameters were investigated, including Mg/Fe coating ratio, $nFe^0@Mg(OH)_2$ dosage, initial pH, reaction temperature, and initial As(V) concentration. The characteristics of the synthesized materials were studied using different techniques, such as transmission electron microscopy (TEM), X-ray diffraction (XRD), and X-ray absorption near edge structure (XANES). Results indicated the superiority of the highest Mg/Fe coating ratio (100%) to the other lower ratios in As(V) removal, corresponding to the adsorption contribution of $Mg(OH)_2$ coating shell. Furthermore, $nFe^0@Mg(OH)_2$-100% could efficiently achieve around 100 % final As(V) removal efficiency at wide pH and temperature ranges (3.0 – 9.0, and 25 – 75 ºC), at a low dosage of 0.5 g/L, reflecting the high applicability of the proposed material. $Mg(OH)_2$ coating enhanced the anti-aggregation effect of the magnetic nanoparticles, which was confirmed by TEM measurements. Kinetics, thermodynamic, and isotherm analyses depicted that pseudo-second-order was the best model to describe the kinetics data, the endothermic nature of the reaction, and a maximum Sips sorption capacity of 89.97 mg/g (following Sips isotherm model), respectively.

K E Y W O R D S

Arsenic (As), Iron nanoparticles (nFe^0), Magnesium hydroxide coating, Reaction conditions, Removal mechanism.

INTRODUCTION

Water pollution is currently the main concern worldwide, whether in developed or developing countries, especially with the continued population inflation accompanied by the continuously increasing water demand. Rapid urbanization and the associated intensive non-eco-friendly disposal of industrial wastes are the primary causes of heavy metals release into either surface or subsurface water [1].

Subsequently, the quality of water and soil is deteriorated by the presence of combinations of such contaminants. For several decades, arsenic (As) contamination of water was considered an issue of great concern. Arsenic is a highly toxic heavy metal that has the potential to cause severe effects on human health, animals, and the environment [2]. Arsenic occurrence in water is associated with either natural causes, including sedimentary and volcanic deposits, or human-made causes, such as industrial and

mining activities. Arsenate (As(V)) is the predominant arsenic species in oxygenated aqueous environments (e.g., AsO_4^{3-}, $HAsO_4^{2-}$, and $H_2AsO_4^{-}$), while arsenite (As(III)) mainly exists as non-ionic $H_3AsO_3^{-}$ in anaerobic environments [3]. Additionally, arsenic is considerably toxic in its inorganic forms which has high carcinogenic effect on humans. Long-term exposure to contaminated water with high As concentration increases the risk of cardiovascular system diseases and skin lesions [1,4]. Accordingly, the World Health Organization (WHO) set arsenic maximum concentration limit in drinking water of 10 µg/L [4].

Nanotechnology has emerged recently in several environmental remediation aspects owing to the excellent functional characteristics of the nanomaterials [5,6]. Iron nanoparticles (nFe^0) have been widely investigated for arsenic removal from water, owing to their high redox potential ($E^0 = -0.44$ V), high reactivity, and large specific surface area (resulted from the nano-size < 100 nm) [7]. Therefore, nFe^0 can treat water from arsenic species, as different mechanisms are involved, including reduction, adsorption, and co-precipitation [8]. Correspondingly, nFe^0-based materials have high reactivity towards most of the inorganic forms of almost all the occurred heavy metals in water bodies, including Cr(VI) [9,10], Zn(II) [11], Pb(II) [12,13], Cd(II) [14], and especially towards As(V) [15]. However, nFe^0 suffers from issues such as the aggregation of the magnetic particles and poor mobility, which limit its applicability in the water treatment field. Hence, modifying the nFe^0 surface by either doping, coating, or supporting can help overcome such issues. Meanwhile, in our previous work, surface coating of nFe^0 with magnesium hydroxide ($Mg(OH)_2$) immensely helped in overcoming several drawbacks from which nFe^0 suffers, including poor mobility, particles aggregation, non-stabilized aqueous suspension, and rapid corrosion of the iron core [7]. Additionally, it showed great removal performance towards Cr(VI) achieving 100% removal performance of 20 mg/L initial Cr(VI) concentration, which was maintained for long reaction time [16]. The non-magnetic, non-toxic, low cost features of $Mg(OH)_2$ makes it one of the perfect candidates as a coating material for nFe^0. Besides, the adsorption abilities of $Mg(OH)_2$ towards different contaminants can be another motivation to be incorporated in nFe^0-based sorbents.

Serval reported studies investigated the efficiency of As removal from water by either bare or modified nFe^0, in which nFe^0-based materials showed a significant potential [3,17,18]. Nevertheless, there is a lack of reported work concerning the use of magnesium hydroxide-coated iron nanoparticles ($nFe^0@Mg(OH)_2$). As shown in **Fig. 1**, the bibliometric analysis of the past decade's published data on arsenic removal by nFe^0-based materials clearly depicted the cruciality of such a research trend. However, the absence of the reported studies on using $nFe^0@Mg(OH)_2$-like materials confirmed the relevant knowledge gap in the literature.

Hence, the main aim of this study is to investigate the potential of $Mg(OH)_2$ coated iron nanoparticles ($nFe^0@Mg(OH)_2$) in improving arsenic removal from aqueous solutions. A set of batch tests has been conducted to understand the effect of several reaction factors, including coating ratio optimization, dosage, initial pH, temperature, and initial As(V) concentration. Furthermore, transmission electron microscopic (TEM) coupled with energy dispersive X-ray (EDX), X-ray diffraction (XRD), and X-ray absorption near edge structure (XANES) were used for the determination of the characteristics of the fresh and spent materials. Additionally, kinetic, isotherm, and thermodynamic analyses were considered for further elaboration of the proposed removal mechanisms of arsenic by $nFe^0@Mg(OH)_2$.

Fig. 1. Bibliometric map of arsenic removal by nFe^0-based materials related keywords occurrence in the literature (Web of Science database, 2012-2022).

EXPERIMENTAL

Chemicals

Ferric chloride ($FeCl_3$, 99.0%, Junsei Chemical Co., Japan), sodium borohydride ($NaBH_4$, 98.0%, Sigma–Aldrich Inc., USA), magnesium nitrate hexahydrate ($Mg(NO_3)_2 \cdot 6H_2O$, > 99.0%, Sigma-Aldrich Inc., USA), disodium hydrogen arsenate ($Na_2HAsO_4 \cdot 7H_2O$, 98.0%, Sigma–Aldrich Inc., USA), sodium hydroxide (NaOH, > 97.0%, Wako Co., Japan), hydrochloric acid (HCl, 30.0%, Wako Co., Japan), ethanol (C_2H_5OH, > 99.5%, Wako Co., Japan), and deionized water (DIW, 18.2 MΩ·cm, Milli-Q filter). All chemicals were procured in analytical grade and directly used without any premodification.

Material synthesis

nFe^0 was prepared via the chemical reduction of $FeCl_3$ precursor by $NaBH_4$ reductant, following the exact synthesis conditions reported in our previous work [19-21]. $nFe^0@Mg(OH)_2$ was synthesized by the thermal deposition of Mg^{2+} precursor on nFe^0 surface via OH^- linking within

Adv. Mater. Lett. | Issue (April-June) 2023, 23021721

[2 of 10]

ethanol medium at 50 ± 1.0 °C [16,22]. Ultrasonication and nitrogen gas purging were considered during the whole synthesis time to ensure the dispersion of the particles within the aqueous media and the anaerobic environment, respectively [23,24]. After an aging time of 1 hour, the formed $nFe^0@Mg(OH)_2$ were separated using 0.2 μm membrane using a vacuum filtration system. Different coating ratios were considered based on Mg/Fe mass ratios of 25%, 50%, and 100%.

Characterization

Different characterization techniques were considered for investigating the physic/chemical characteristics of the synthesized materials. Transmission electron microscopy coupled with energy dispersive X-ray spectroscopy (TEM-EDS, JEM-ARM 200F, JEOL Co., Japan) was used to examine the morphological features and the surface composition. X-ray diffraction (XRD, TTR, Rigaku Inc., Japan) was used to determine the structural and crystallographic properties. X-ray absorption near edge structure (XANES) measurements of As K-edge in fluorescence model using beamline 27B at the Photon Factory (KEK, Tsukuba, Japan) were conducted for the determination of the nature of sorbent/sorbate interaction as well as the oxidation states of the loaded arsenic species on the spent $nFe^0@Mg(OH)_2$.

Reaction & analysis

Batch experiments were conducted to evaluate the efficiency of $nFe^0@Mg(OH)_2$ in As(V) removal from aqueous solutions. Several reaction conditions were investigated, in the exact following sequence, including Mg/Fe coating ratio (25%, 50%, and 100%), $nFe^0@Mg(OH)_2$ dosage (0.2, 0.5, 1.0, and 2.0 g/L), initial pH (3.0, 5.0, 7.0, 9.0 and 12.0), reaction temperature (25, 35, 55, and 75 °C), and initial As(V) concentration (5, 10, 20, and 40 mg/L). The baseline conditions for the reaction parameters optimization were initial As(V) concentration of 20 mg/L, initial pH of 5.0 ± 0.2, and reaction temperature of 25 ± 1.0 °C. Water samples were periodically withdrawn over 120 min reaction time to be analyzed for As(V) concentration using an inductively coupled plasma mass spectrometer (ICP-MS, Agilent-7500cx, Agilent Tech., USA). As(V) removal efficiency and adsorption capacity were calculated according to the following equations [25]:

$$\text{Removal efficiency (R\%)} = \frac{C_0 - C_t}{C_0} \times 100 \qquad (1)$$

$$\text{Adsorption capacity (}q_e\text{)} = \frac{(C_0 - C_e)\,V}{m} \qquad (2)$$

where C_0 (mg/L), C_t (mg/L), and C_e (mg/L) denote the initial, time (t)-corresponding, and equilibrium As(V) concentrations, respectively. V is the solution volume (L), and M stands for the mass of $nFe^0@Mg(OH)_2$ adsorbent (g).

Data modelling

To evaluate the adsorption kinetics behaviour of As(V) removal by $nFe^0@Mg(OH)_2$, the experimental data are fitted using the pseudo-first-order, pseudo-second-order, intra-particle diffusion, and Elovich models, respectively [26-29].

Pseudo-first-order model:
$$q_t = q_e\,(1 - e^{-k_1 t}) \qquad (3)$$

Pseudo-second-order model:
$$q_t = \frac{q_e^2 k_2 t}{1 + q_e k_2 t} \qquad (4)$$

Intra-particle diffusion model:
$$q_t = k_{int} t^{0.5} + C_{int} \qquad (5)$$

Elovich model:
$$q_t = \frac{1}{\beta}\ln(\alpha \beta t + 1) \qquad (6)$$

where q_t (mg/g) represents the amount of As(V) adsorbed by a mass unit of $nFe^0@Mg(OH)_2$ at a predetermined time t (min); k_1 (1/min) is the pseudo-first-order adsorption rate constant; k_2 (g/mg min) is the pseudo-second-order adsorption rate constant; k_{int} (mg/g min$^{0.5}$) is the intra-particle diffusion rate constant; C_{int} (mg/g) is a constant that represents the boundary layer thickness, β (mg/g min) is Elovich initial adsorption rate constant, and α (g/mg) is Elovich adsorption rate constant.

To predict the adsorption mechanism, investigations on adsorption thermodynamics are crucial. The thermodynamic parameters were determined via the following equations [30-32].

$$\Delta G = -RT \ln K_d \qquad (7)$$
$$\Delta G = \Delta H - T\Delta S \qquad (8)$$
$$\ln K_d = \Delta S/R - \Delta H/RT \qquad (9)$$

where ΔG is Gibbs free energy change (kJ/mol), ΔH is enthalpy change (kJ/mol), ΔS is entropy change (J/mol Kelvin), T is the temperature in Kelvin, and R is the universal gas constant (8.314 J/mol Kelvin), When plotted against q_e, the curve intercept of $\ln(q_e/C_e)$ yields the thermodynamic equilibrium constants K_d.

Adsorption isotherm curves are useful for analyzing the interaction between adsorbent and adsorbate as well as the properties of the adsorption layer. The Langmuir, Freundlich, and Sips (modified Langmuir/Freundlich) adsorption isotherm models are described as the following equations, respectively [26,33,34].

Langmuir isotherm model:
$$q_e = \frac{q_{\max(L)} K_L C_e}{1 + K_L C_e} \qquad (10)$$

Separation factor:
$$R_L = \frac{1}{1 + K_L C_0} \qquad (11)$$

Freundlich isotherm model:
$$q_e = K_F C_e^{1/n} \qquad (12)$$

Sips isotherm model:
$$q_e = \frac{q_{\max(s)} K_S C_e^{n_S}}{1 + K_S C_e^{n_S}} \qquad (13)$$

where $q_{\max(L)}$ (mg/g) stands for Langmuir maximum adsorption capacity; The Langmuir constant associated with adsorption energy is K_L (L/mg); The separating factor is R_L: $R_L = 1$, linear; $R_L = 0$, irreversible; $R_L > 1$, unfavorable; $0 < R_L < 1$, favorable. K_F is the Freundlich

OPEN ACCESS

constant [(mg/g) (L/mg) $^{1/n}$], while $1/n$ is the adsorption affinity constant.

The coefficient of determination (R^2) was used to determine the best-fitting models. Moreover, the well-known Akaike Information Criterion (AIC) model was considered for investigating the goodness of fit for all the applied models [32,35,36]:

$$AIC = 2K + N \ln \left[\frac{SSE}{N} \right] + \frac{2K(K+1)}{N-K-1} \qquad (14)$$

where K is the number of the independently adjusted parameters in the applied model, N is the number of experimental measurements, and SSE is the sum of squared errors between the experimental (q_{exp}) and calculated (q_{calc}) equilibrium adsorption capacities, which can be estimated by the following formula.

$$SSE = \sum_i^N (q_{exp} - q_{calc})_i^2 \qquad (15)$$

The lower the AIC value, the better the fitting of the model to the experimental data. So, the model with the lowest AIC value shall be chosen to describe the data.

It is worth mentioning that non-linear modeling was considered for the kinetic and isotherm modeling as it showed higher accuracy and to avoid the errors resulting from non-linear/linear transformation in terms of error structure, error variance, and normality assumptions of the standard least squares [29,37].

RESULTS AND DISCUSSION

Materials characterization

XRD patterns of fresh and reacted material are displayed in **Fig. 2**. Fresh nFe^0 exhibited the two typical characteristic peaks of α-Fe^0 at 2θ of 44.8° and 82.16°, confirming the presence of the pure iron core. The freshly prepared Mg(OH)$_2$ showed a mixture of crystalline and amorphous peaks, attributed to MgO (ICSD, Code: 31053), and brucite (ICSD, Code: 31053), respectively [38]. XRD pattern of fresh nFe^0@Mg(OH)$_2$ (100% coating ratio) showed a lower-intensity peak of α-Fe^0, owing to the high Mg/Fe coating ratio and the moderate amorphous nature of the Mg(OH)$_2$ coating. Such a phenomena was less observed in lower coating ratios, as previously reported [16,22]. Furthermore, the coating layer successfully protected the iron core from rapid oxidation, reflected by the absence of iron oxide peaks. Such a hypothesis was confirmed by X-ray photoelectron spectroscopy analysis (XPS) which was conducted in our previous work [16]. XPS analysis was conducted for the freshly synthesized nFe^0 and nFe^0@Mg(OH)$_2$ (100% coating ratio) (**Fig. S1, supporting information**). The presence of iron oxide (II/III) states in addition to Fe^0 states was confirmed in the Fe 2p region at a binding energy range of 706 – 726 eV, indicating the high sensitivity of the freshly synthesized nFe^0 to corrosion. The presence of iron oxide states could be related to the possible oxidation during the sample preparation for XPS analysis, owing to the extreme reactivity of the freshly synthesized nFe^0. Whereas the surface of nFe^0@Mg(OH)$_2$ was completely clear from any iron oxidation states, reflecting

the protection of the iron core. Additionally, the O 1s region showed further confirmation of the absence of any metal oxide states, besides the explicit attribution of Mg(OH)$_2$ coating on the surface (corresponding to M—OH).
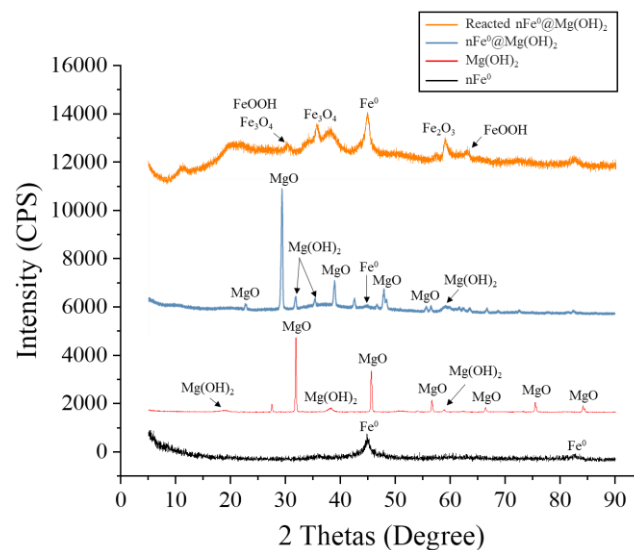
Fig. 2. XRD patterns of fresh and reacted materials.

In the case of the reacted nFe^0@Mg(OH)$_2$, XRD patterns depicted the presence of magnetite, maghemite, and iron oxide-hydroxide on the particle's surface after the reaction with As(V), indicating the possible involvement of adsorption and co-precipitation in As removal process [39]. Nevertheless, it was clearly observed that α-Fe^0 peak was maintained even after the reaction, which confirmed the protective effect of the Mg(OH)$_2$ coating, which prevented the rapid corrosion of the iron core. Hence, it can be concluded that the iron core could be partially oxidized, achieving the multi-function al aim of removing As sufficiently and protecting the iron core (the electron source) for prolonged reactive performance.

TEM imaging of nFe^0 and nFe^0@Mg(OH)$_2$ (100% coating ratio) is shown in **Fig. 3**. Fresh nFe^0 yielded the typical chain-like aggregated morphology with an average particle size ranging from 30 to 60 nm. For nFe^0@Mg(OH)$_2$, the irregularly shaped clouds of Mg(OH)$_2$ were clearly observed around the black spherical iron particles. Such observations were confirmed by the EDS elemental mapping, which exhibited the uniform distribution of Mg and O, and the concentration of Fe inside the black iron core. It is worth mentioning that H, as a light element, was not detected in EDS analysis. nFe^0@Mg(OH)$_2$ showed a slightly finer particle size than nFe^0, with an average particle size ranging from 25 to 50 nm. The anti-aggregation effect of the non-magnetic Mg(OH)$_2$ coating enhanced the discreteness of the particles to some extent compared with that of nFe^0, showing less overlapping of the spherical particles. However, further sonication of the samples before TEM measurements could have led to enhanced dispersion of the particles over the TEM grid.

Adv. Mater. Lett. | Issue (April-June) 2023, 23021721

[4 of 10]
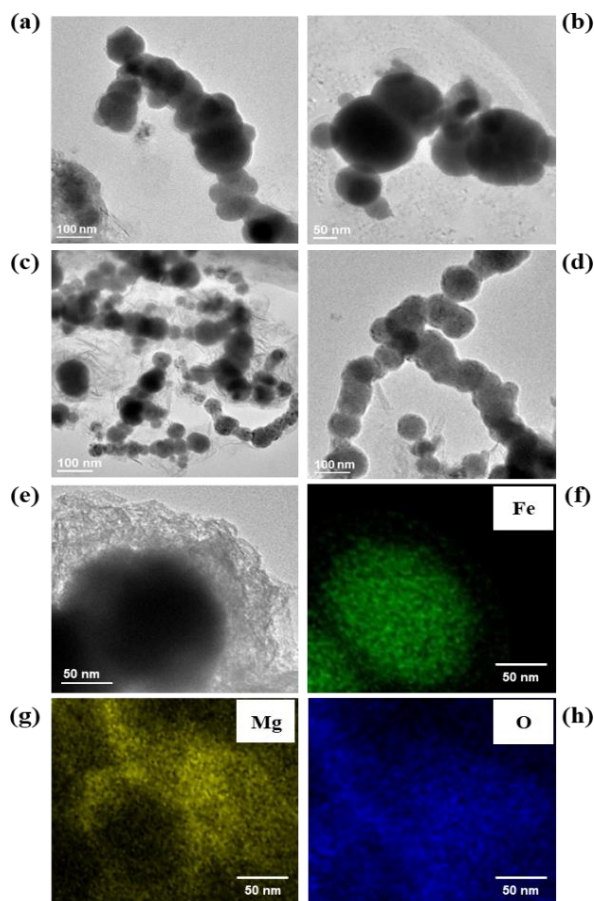
Fig. 3. TEM imaging at different magnification values of nFe^0 (a) and (b), $nFe^0@Mg(OH)_2$ (c) and (d), and TEM-EDS elemental mapping of $nFe^0@Mg(OH)_2$ (e), (f), (g), and (h).

As(V) removal results

Batch experiments were conducted to evaluate the efficiency of $nFe^0@Mg(OH)_2$ in As(V) removal from aqueous solutions. The first step was optimizing the Mg/Fe coating ratio (25%, 50%, and 100%), considering $nFe^0@Mg(OH)_2$ dosage of 1.0 g/L. As shown in **Fig. 4(a)**, such a dosage of either nFe^0 or $nFe^0@Mg(OH)_2$ was enough to achieve full removal within just 5 min of the reaction time, which was auspicious results; taking into consideration the initial As(V) concentration of 20 mg/L is much higher than the normally detected range in water bodies [**40,41**]. Hence, it was necessary to consider a lower dosage (0.5 g/L) to study the actual difference between the bare and the coated nFe^0 in As(V) removal.

Results indicated that the higher Mg/Fe coating ratio, the more enhanced As(V) removal was observed, corresponding to final As(V) concentrations of 3.1, 0.8, and 0.001 mg/L for 25, 50, and 100% coating ratios, respectively (**Fig. 4(b)**). Such results implied the contribution of $Mg(OH)_2$ coating shell in adsorbing As(V) aqueous species, which can be attributed to the electrostatic attraction between the negatively charged A(V) species to the positively charged surface of $nFe^0@Mg(OH)_2$, which was confirmed by improved As(V) removal comparing

with that of nFe^0. The superiority of nFe^0 to $nFe^0@Mg(OH)_2$ (25 and 50% coating ratios) could be related to several attributions; (1) the rapid release of electrons from the iron core was favorable in the case of nFe^0, yielding faster and higher As(V) reduction to As(III), compared to that of $nFe^0@Mg(OH)_2$ (25 and 50% coating ratios). (2) 25 and 50% coating ratios could have contributed to As(V) adsorption, yet not comparable to that high coating ratio (100%). (3) the dominant removal mechanism at the early stage of the reaction is reduction (favoring nFe^0), while at later stages, adsorption and co-precipitation are involved (which can occur in all nFe^0 materials, either bare or coated). However, the low-moderate solubility of $Mg(OH)_2$ coating shell caused a moderate release of Mg and Fe cations, unlike $nFe^{0,}$ which rapidly oxidized, indicating the higher contribution of the adsorptive sites in As(V) removal in the case of nFe^0. Meanwhile, the adsorptive positively charged sites of $Mg(OH)_2$ increased at a higher coating ratio (100%), causing the showed competitive performance to that of nFe^0. Hence, $nFe^0@Mg(OH)_2$ with 100% coating ratio was optimal for further reaction conditions investigation. It is worth mentioning that the obtained As(V) removal performance by nFe^0 prepared in this study is remarkably higher than most of the reported studies, which can be attributed to two reasons; (1) most of the reported nFe^0 in the studies are either commercial (lower reactivity than the experimentally synthesized) or in micro-size (lower reactivity and specific surface area than nano-size). (2) the present nFe^0 was prepared according to a previously conducted optimization of all the synthesis conditions (e.g., precursor concentration, reductant concentration, reductant solution volume, pH, mixing rate, temperature, etc.), which was reported in our previous work [**42**], yielding higher reactivity towards contaminants.
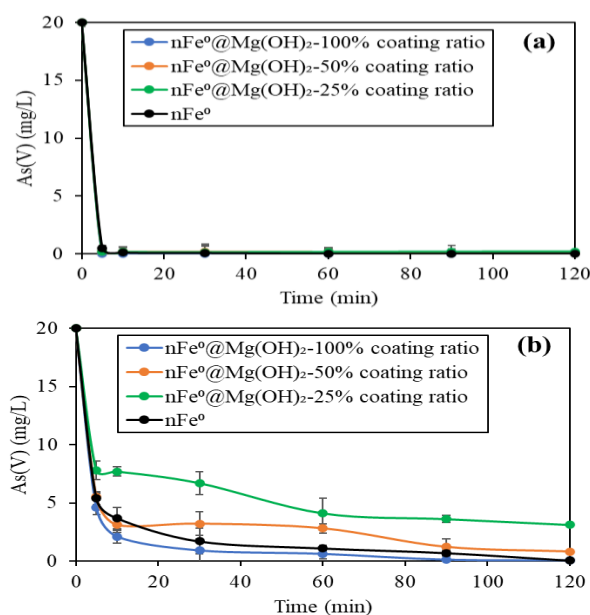

Fig. 4. Optimization of Mg/Fe coating ratio towards As(V) removal for two different $nFe^0@Mg(OH)_2$ dosages: (a) 1.0 g/L, and (b) 0.5 g/L.

Adv. Mater. Lett. | Issue (April-June) 2023, 23021721

[5 of 10]

Investigating different dosages of nFe^0@Mg(OH)$_2$-100% (0.25 – 2.0 g/L) for As(V) removal showed that even at the lowest dosage (0.25 g/L) around 98% final As(V) removal efficiency was achieved, indicating that there is no need for high dosages (> 1.0 g/L) to reach a feasible and sufficient As(V) removal performance (**Fig. 5(a)**). Hence, 0.5 g/L was selected as the optimal dosage as it achieved a final As(V) removal efficiency of around 99.8%. It should be mentioned that investigating the reaction conditions using 1.0 g/L nFe^0@Mg(OH)$_2$ dosage was conducted, and results have not shown any observed changing trends, owing to the ability of such dosage to fully remove As(V) at almost all the conditions (**Fig. S2, supporting information**).

The effect of initial pH was studied, considering a pH range from 3.0 to 12.0. As shown in **Fig. 5(b)**, As(V) removal was significantly induced at the strong acidic conditions, unlike the strong alkaline, which was significantly observed at the early stages of the reaction (5 – 30 min). Such observations can be attributed to the following reasons: (1) the strong acidic pH conditions induced the dissolution of Mg(OH)$_2$ coating shell in water, which has a moderate solubility, thereby exposing the nFe^0 core to the rapid corrosion, (2) the release of electrons from nFe^0 core at acidic conditions is higher than that at alkaline conditions, thus As(V) reduction to As(III) would be enhanced at acidic conditions, and (3) the role of electrostatic sorption of negatively charged As(V) species to the positively charged surface of nFe^0@Mg(OH)$_2$ would fade approaching towards the strong alkaline conditions (pH 12.0), knowing that the point of zero charge of the material was estimated to be 11.6 (negatively charged > pH: 11.6, and positively charged < pH: 11.6) [16,29].
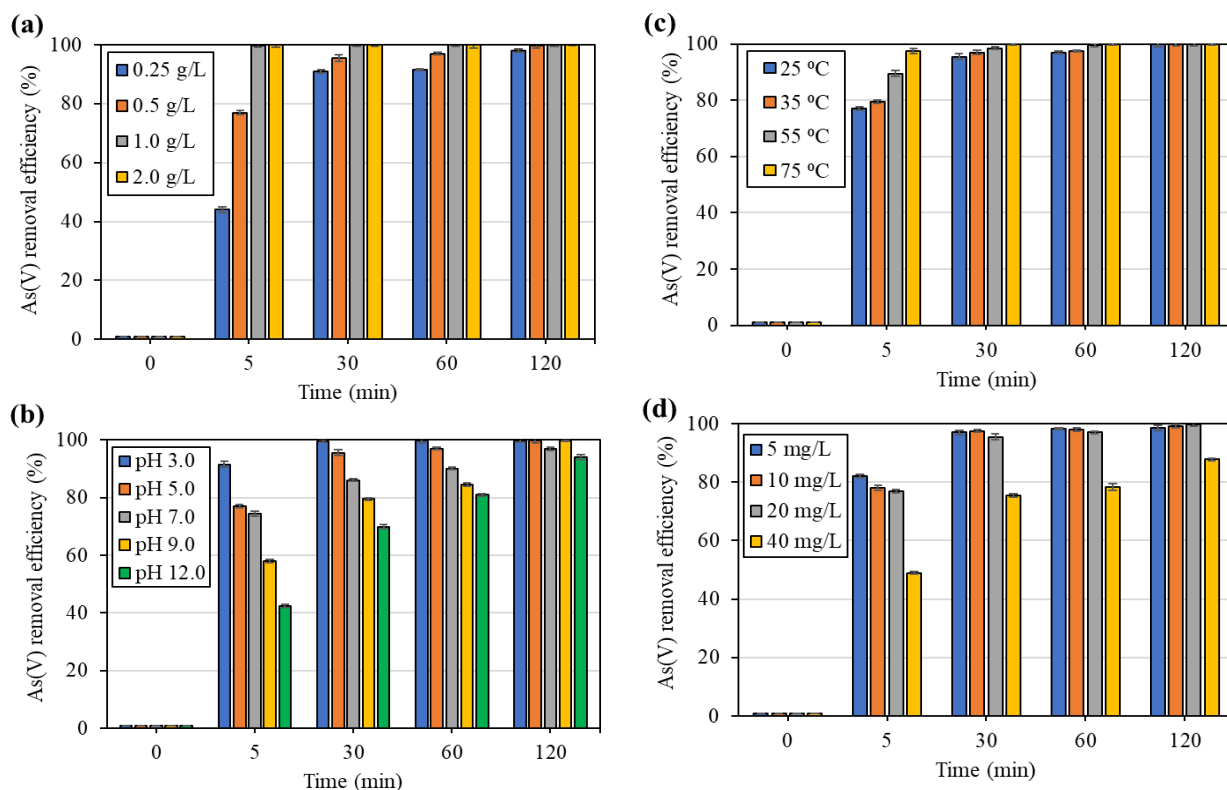
Fig. 5. Effect of nFe^0@Mg(OH)$_2$ dosage (a), initial pH (b), reaction temperature (c), and initial As(V) concentration (d) on As(V) removal by nFe^0@Mg(OH)$_2$-100%.

It is worth mentioning that, despite the presumed strong affinity between the dominant As(V) species at alkaline conditions (HAsO$_4$$^{2-}$ > pH 7.0, and H$_2$AsO$_4$$^-$ < pH 7.0) and the positively charged surface of nFe^0@Mg(OH)$_2$, the change of the surface charge of the material from positive to negative at pH 12.0 diminished the electrostatic sorption role, causing As(V) removal efficiency to be the lowest at pH 12.0. XANES measurements were conducted to As loading on the reacted nFe^0@Mg(OH)$_2$ materials at different pH and temperature values (**Fig. 6**). The resulting As K-edge XANES spectra for all the reacted samples confirmed As(V) adsorption and the absence of As(III) [43], which could be related to two attributions: (1) the role of As(V) sorption can be comparable to the reduction of As(V) to As(III), owing to the aforementioned electrostatic sorption phenomena, Mg(OH)$_2$ sorption abilities, and As(V) uptake by the formed FeOOH, (2) the possible oxidation of the As(III) traces in the reacted materials within the samples preparation for XANES measurements.

Adv. Mater. Lett. | Issue (April-June) 2023, 23021721

[6 of 10]
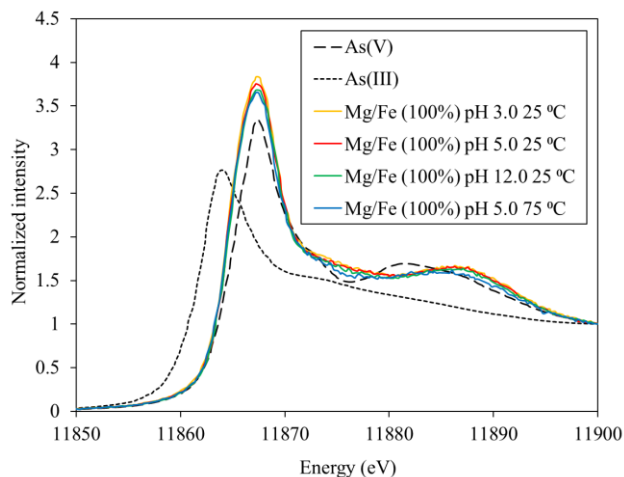
Fig. 6. As K-edge XANES spectra for standard As(V) and As(III) and adsorbed As on $nFe^0@Mg(OH)_2$ at different pH and temperature conditions.

The adsorption kinetic rates of $nFe^0@Mg(OH)_2$ for As(V) removal were investigated using four models; pseudo-first-order, pseudo-second-order, intraparticle diffusion, and Elovich models (**Table S1, supporting information**). In terms of kinetic characteristics, compared with the correlation coefficient (R^2) and AIC values, the best fitting model was exchanged between the pseudo-first-order model and the pseudo-second-order, with a slight superiority to the later, indicating that the pseudo-second-order model can better describe the adsorption reaction and chemisorption mainly control the adsorption process. Nevertheless, the clear competition from the pseudo-first-order model depicted the possible involvement of the physisorption adsorption process, represented by the aforementioned As(V) sorption pathways. The observations of kinetic rate constant values indicated that the kinetic rate of As(V) sorption increased by the decrease of the initial pH and the increase of the reaction temperature.

The effect of reaction temperature was investigated by considering a range from 25 to 75 ℃. As displayed in **Fig. 5(c)**, it was clear that increasing the reaction temperature resulted in enhancing As(V) removal efficiency, achieving full removal at 35, 55, and 75 ℃. Nevertheless, even at 25 ℃, $nFe^0@Mg(OH)_2$ could still achieve a final As(V) removal efficiency of 99.8%, implying the practicality of the proposed $nFe^0@Mg(OH)_2$ without the need for high reaction temperature to reach sufficient As(V) removal. Thermodynamic analysis represents the cornerstone for understanding the effect of reaction temperature on the adsorption process mechanism. According to **Table 1** and **Fig. S3 (supporting information)**, the positive sign of enthalpy change ($\Delta H > 0$) at different reaction temperatures, demonstrated that As(V) adsorption on $nFe^0@Mg(OH)_2$ has an endothermic nature and that the adsorption process is favored at higher temperatures [**26**]. Furthermore, the

positive sign of entropy change ($\Delta S > 0$), indicated the irreversibility of the adsorption process and the increase of the free energy within the aqueous system [**26**]. Additionally, the negative sign of the change in Gibbs free energy ($\Delta G < 0$) indicated the spontaneity of the adsorption process [**34**]. The values of the change in Gibbs free energy implied that As(V) removal by $nFe^0@Mg(OH)_2$ is governed by physisorption, indicating the significant role of electrostatic sorption in the process. Moreover, the magnitude of enthalpy change ($\Delta H = 145.69$ kJ/mol) suggested that the removal mechanism also involves a chemisorption process, which can be attributed to As(V) reduction to As(III) and the possible co-precipitation of As(III) with the released Fe^{2+}.

Table 1. Thermodynamic parameters of As(V) removal by $nFe^0@Mg(OH)_2$.

Temperature (Kelvin)	$\triangle G$ (kJ/mol)	$\triangle H$ (kJ/mol)	$\triangle S$ (J/mol Kelvin)
298.15 (25 ℃)	-11.263	145.69	528.11
308.15 (35 ℃)	-17.697		
328.15 (55 ℃)	-27.628		
348.15 (75 ℃)	-37.983		

The initial concentration effect on As(V) removal by $nFe^0@Mg(OH)_2$ was studied considering different values (5, 10, 20, and 40 mg/L). The results clearly indicated the potential of $nFe^0@Mg(OH)_2$ to satisfactorily remove As(V), even at extreme As(V) concentrations, where it exhibited final removal efficiency of around 88% of 40 mg/L initial As(V) concentration (**Fig. 5(d)**). While at lower initial concentrations, much better removal performance was observed. Adsorption isotherm models were used to further investigate the As(V) removal mechanism. As exhibited in **Table 2** and **Fig. S4 (supporting information)**, the Sips isotherm model had more significant correlation coefficient (R^2) than that of Langmuir or Freundlich isotherm models (despite the higher AIC value), indicating that the adsorption process involves both physisorption and chemisorption, and As(V) sorption on $nFe^0@Mg(OH)_2$ can be executed as a multi- or mono-layer adsorption. Such results agreed with the aforementioned interpretations for kinetics and thermodynamic analyses. Additionally, the parameter (n) of the Freundlich model was higher than 1, indicating the strong affinity between As(V) species and $nFe^0@Mg(OH)_2$ surface [**26**]. Meanwhile, the separation factor R_L calculated by the Langmuir model was in the range from 0 to 1, verifying that the adsorption process occurs in a profitable orientation (**Table S2, supporting information**) [**26**]. Furthermore, $nFe^0@Mg(OH)_2$ exhibited a maximum sorption capacity to As(V) of 89.97 mg/g (from Sips isotherm model), which was higher than most of the previously reported iron-based sorbents (**Table S3, supporting information**).

Adv. Mater. Lett. | Issue (April-June) 2023, 23021721

[7 of 10]

Table 2. Adsorption isotherm parameters of As(V) removal by $nFe^0@Mg(OH)_2$.

Isotherm model	Parameter (unit)	Value
Langmuir	K_L (L/mg)	2.55
	$q_{max(L)}$ (mg/g)	74.42
	R^2	0.988
	AIC*	23.85
Freundlich	K_F [(mg/g) (L/mg) $^{1/n}$]	41.89
	n	2.98
	R^2	0.986
	AIC*	24.56
Sips	K_s (L/g)	1.18
	n_s	0.68
	$q_{max(s)}$ (mg/g)	89.97
	R^2	0.993
	AIC*	26.75

*Akaike Information Criterion

Practical features

The effect of ionic strength on the reactive performance of $nFe^0@Mg(OH)_2$ was investigated, considering different $NaNO_3$ concentrations (0.001, 0.01, 0.1, and 1.0 M). Results indicated that As(V) removal by $nFe^0@Mg(OH)_2$-100% was not significantly influenced by the change in the ionic strength of the solution (up to 0.1 M), showing a slight decrease of final As(V) removal efficiency (maximum 4.7% for 0.1 M) (**Fig. S5, supporting information**). For the highest ionic strength (1.0 M), As(V) final removal efficiency showed 10.8% difference less than the normal conditions. At higher ionic strengths, electrostatic repulsion between the reactive colloids can be reduced allowing more effective solid/liquid interaction, thus attributing the comparable As(V) removal [**44**]. Such results implied that the proposed $nFe^0@Mg(OH)_2$ can efficiently remove As(V) from aqueous solutions within a wide range of ionic strength. In terms of practicality, the investigated ionic strength range confirmed the possibility of employing $nFe^0@Mg(OH)_2$ in As(V) water treatment applications from either waste streams or groundwater [**45,46**].

The storage stability of nanomaterials is a crucial factor that governs their practicality in water treatment field. Hence, storage stability of the synthesized $nFe^0@Mg(OH)_2$-100% was studied considering various storing conditions, including no storing solution (exposed to air), no storing solution, storing in ethanol, and storing in deionized water (DIW). As(V) removal performance of the stored materials was tested after a shelf-time of 1.0 day (**Fig. S6, supporting information**). Results showed no significant deterioration in As(V) removal efficiency in most of the storing conditions, except for the one exposed to air. After 1.0 day shelf-time, the stored $nFe^0@Mg(OH)_2$ achieved final removal efficiency of 90.8, 93.0, and 89.9% for the no-storing, ethanol-storing, and DIW-storing conditions, respectively. The exposure of the material to air without any preserving solution caused around 19% decrease in the final removal efficiency compared with that of the freshly synthesized material. We believe that $Mg(OH)_2$ coating shell managed to protect the iron core even at air-exposing conditions, which was reflected by the

reasonable As(V) removal after a long shelf-time (1.0 day). However, the observed visual deformation in the total size of the material as well as the hardness of the material affected the dispersion of the material in the reaction solution, thus influencing As(V) removal (especially at the early stages of the reaction). The obtained results were in great agreement with our previously reported findings concerning Cr(VI) removal by $nFe^0@Mg(OH)_2$, considering much longer shelf-time (up to 30 days) [16..

Removal mechanism

The suggested pathways of As(V) removal process by $nFe^0@Mg(OH)_2$ can be summarized as follows:

- Oxidation of nFe^0 to form Fe^{3+} and Fe^{2+} [**47,48**].
$$2Fe^0 + 2H_2O \rightarrow 2Fe^{2+} + H_2 + 2OH^- \quad (16)$$
$$2Fe^0 + O_2 + 2H_2O \rightarrow 2Fe^{2+} + 4OH^- \quad (17)$$
$$4Fe^0 + 3O_2 + 2H_2O \rightarrow 4\gamma - FeO(OH) \quad (18)$$
$$Fe^{2+} \xrightarrow{O_2} Fe^{3+} \quad (19)$$

- As(V) reduction to As(III) by the released electrons from nFe^0 core, followed by As(III) reduction to As^0 [**49-52**].
$$2HAsO_4^{2-} + 2Fe^0 + 6H^+ \rightarrow 2Fe^{2+} + 2H_2AsO_3^- + 2H_2O \quad (20)$$
$$2H_2AsO_3^- + 2Fe^0 + 2H^+ \rightarrow Fe_2O_3 + 2As^0 + 3H_2O \quad (21)$$

- As(III) co-precipitation with the released Fe^{2+} and As(V) adsorption on the formed iron oxide-hydroxide shell [**3,49**].
$$2H_2AsO_3^- + Fe^{2+} = FeAs_2O_4 + 2H_2O \quad (22)$$
$$HAsO_4^{2-} + Fe - OH + H^+ = FeHAsO_4 + H_2O \quad (23)$$

- Electrostatic attraction of the negatively charged As(V) species to the positively charged surface of $nFe^0@Mg(OH)_2$ [**16**].
$$HAsO_4^{2-} + Fe^0@Mg(OH)_2 \rightarrow As(V) \equiv Mg(OH)_2 \quad (24)$$

Therefore, it could be implied that oxidation, reduction, surface adsorption, and chemical co-precipitation are involved as complex removal mechanisms for As(V) removal from water using $nFe^0@Mg(OH)_2$.

CONCLUSION

In this study, $nFe^0@Mg(OH)_2$ was used for As(V) removal from aqueous solutions. Coating the magnetic nFe^0 particles with the non-magnetic non-toxic $Mg(OH)_2$ coating resulted in an enhanced anti-aggregation effect, which was confirmed by the well-distributed $Mg(OH)_2$ clouds around the black nFe^0 core from TEM-EDS measurements. The protecting effect of the coating material exhibited a slower corrosion rate of the iron core, which was depicted from XRD patterns. The results of reaction conditions optimization showed the great potential of $nFe^0@Mg(OH)_2$ with the coating ratio 100% to efficiently remove As(V) within wide pH and temperature ranges (3.0 – 9.0, and 25 – 75 ºC) at a low dosage of 0.5 g/L. Furthermore, $nFe^0@Mg(OH)_2$ showed the ability to

Adv. Mater. Lett. | Issue (April-June) 2023, 23021721

[8 of 10]

achieve satisfactorily As(V) removal with the extreme initial arsenic concentrations (e.g., 40 mg/L: 88% final removal efficiency). Kinetics modeling indicated that pseudo-second-order model was the best to describe the adsorption reaction rate of As(V) removal by $nFe^0@Mg(OH)_2$. Whereas thermodynamic modeling depicted the endothermic nature of the reaction and the involvement of both physisorption and chemisorption in the removal process. Such implications were confirmed by the adsorption isotherm modeling, which reflected the possibility of multi- and mono-layer sorption to occur within the removal process, following Sips isotherm model. Generally, the obtained results confirmed the great potential of the proposed $nFe^0@Mg(OH)_2$ in As(V) removal from aqueous solutions and suggested its incorporation in the real treatment applications of heavy metals contaminated water as one of the perfect candidates.

ACKNOWLEDGEMENTS

CONFLICTS OF INTEREST

There are no conflicts to declare.

SUPPORTING INFORMATION

Supporting informations are available online at journal website.
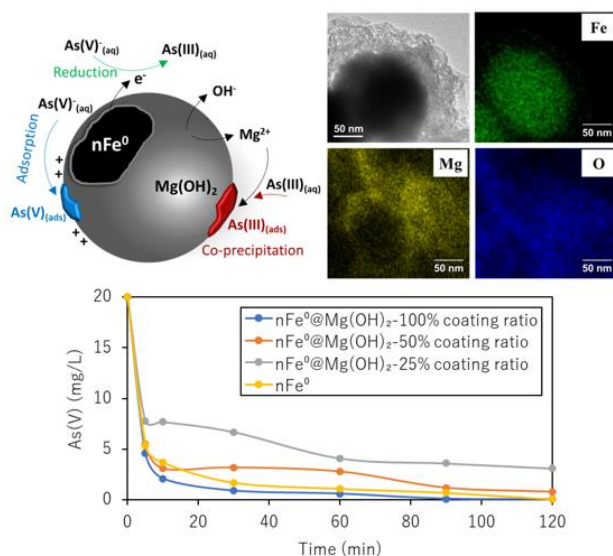
REFERENCES

1. Reddy, A. V. B.; *et al.*, *J. Environ. Chem. Eng.*, **2016**, *4*, 3537.
2. Izah, S. C.; Chakrabarty, N.; Srivastav, A. L.; *Expo. Heal.*, **2016**, *8*, 285.
3. Eljamal, O.; Sasaki, K.; Hirajima, T.; *Appl. Math. Model.*, **2011**, *35*, 5198.
4. W. H. Organization and WHO., *Guidelines for Drinking-Water Quality*, Vol. 1. World Health Organization, **2004**.
5. Ghasemzadeh, G.; Momenpour, M.; Omidi, F.; Hosseini, M. R.; Ahani, M.; Barzegari, A.; *Front. Environ. Sci. Eng.*, **2014**, 8, 471.
6. Zhao, X.; Liu, W.; Cai, Z.; Han, B.; Qian, T.; Zhao, D.; *Water Res.*, **2016**, *100*, 245.
7. Maamoun, I.; Eljamal, O.; Eljamal, R.; Falyouna, O.; Sugihara, Y.; *Appl. Surf. Sci.*, **2020**, *506*, 145018. DOI: https://doi.org/10.1016/j.apsusc.2019.145018.
8. Kanel, S. R.; Grenèche, J.M.; Choi, H.; *Environ. Sci. Technol.*, **2006**, *40*, 2045. DOI: 10.1021/es0520924.
9. Shi, L.; Zhang, X.; Chen, Z.; *Water Res.*, **2011**, *45*, 886.
10. Singh, R.; Misra, V.; Singh, R. P.; *J. Nanoparticle Res.*, **2011**, *13*, 4063.
11. Yan, W.; Herzing, A. A.; Kiely, C. J.; Zhang, W.; *J. Contam. Hydrol.*, **2010**, 118, 96.
12. Zhang, X.; Lin, S.; Chen, Z.; Megharaj, M.; Naidu, R.; *Water Res.*, **2011**, *45*, 3481.
13. Wang, G.; *et al.*, *Chemosphere*, **2014**, *117*, 617.
14. Eglal, M. M.; Ramamurthy, A. S.; *J. Environ. Sci. Heal. Part A*, **2015**, *50*, 901.
15. Ray, P. Z.; Shipley, H. J.; *RSC Adv.*, **2015**, *5*, 29885.
16. Maamoun, I.; *et al.*, *J. Environ. Chem. Eng.*, **2022**, *10*, 107431. DOI: https://doi.org/10.1016/j.jece.2022.107431.
17. Kanel, S. R.; Nepal, D.; Manning, B.; Choi, H.; *J. Nanoparticle Res.*, **2007**, *9*, 725. DOI: 10.1007/s11051-007-9225-7.
18. Giasuddin, A.B.M.; Kanel, S. R.; Choi, H.; *Environ. Sci. Technol.*, **2007**, *41*, 2022.
19. Maamoun, I.; Eljamal, O.; Shubair, T.; Noutsuka, H.; Saha, B.B.;. Matsunaga, N.; "Integrating nano-scale zero valent iron (nZVI) in phosphorus removal from aqueous solution through porous media: packed-column experiment," *Proc. Int. Exch. Innov. Conf. Eng. Sci.*, **2017**, Vol. 3, PP. 25-30.
20. Falyouna, O.; Maamoun, I.; Bensaida, K.; Tahara, A.; Sugihara, Y.; Eljamal, O.; *Water Pract. Technol.*, **2022**, *17*, 75.
21. Maamoun, I.; Eljamal, O.; Thompson, I.; Eljamal, R.; Falyouna, O.; Sugihara, Y.; "Effect of Nano Zero Valent Iron Delivery Method into Porous Media on Phosphorus Removal from Groundwater," *Proc. Int. Exch. Innov. Conf. Eng. Sci.*, **2019**, Vol. 5, PP. 9-11.
22. Maamoun, I.; Falyouna, O.; Eljamal, R.; Idham, M. F.; Tanaka, K.; Eljamal, O.; *Chem. Eng. J.*, **2023**, *451*, 138718.
23. Bensaida, K.; Maamoun, I.; Eljamal, R.; Falyouna, O.; Sugihara, Y.; Eljamal, O.; *Energy Convers. Manag.*, **2021**, *249*, 114877. DOI: https://doi.org/10.1016/j.enconman.2021.114877.
24. Eljamal, R.; Maamoun, I.; Bensaida, K.; Yilmaz, G.; Sugihara, Y.; Eljamal, O.; *Renew. Sustain. Energy Rev.*, **2022**, *158*, 112192. DOI: https://doi.org/10.1016/j.rser.2022.112192.
25. Falyouna, O.; Eljamal, O.; Maamoun, I.; "Removal of Cesium from Contaminated Waters by Employing Iron-Based Nanoparticles and Nanocomposites," in *Proceeding of International Exchange and Innovation Conference on Engineering & Sciences (IEICES)*, 2019, Vol. 5, No. March 2020, PP. 26-27.
26. Maamoun, I.; Eljamal, R.; Falyouna, O.; Bensaida, K.; Sugihara, Y.; Eljamal, O.; *J. Mol. Liq.*, **2021**, 115402.
27. Wu, F. C.; Tseng, R. L.; Juang, R. S.; *Chem. Eng. J.*, **2009**, *153*, 1. DOI: 10.1016/j.cej.2009.04.042.
28. Aharoni, C.; Sparks, D. L.; "Kinetics of soil chemical reactions. A theoretical treatment," *SSSA Spec. Publ. (Soil Sci. Soc. Am.*, **1991**, No. 27, PP.1-18. DOI: 10.2136/sssaspecpub27.c1.
29. Falyouna, O.; Maamoun, I.; Bensaida, K.; Tahara, A.; Sugihara, Y.; Eljamal, O.; *J. Colloid Interface Sci.*, **2022**, *605*, 813. DOI: https://doi.org/10.1016/j.jcis.2021.07.154.
30. Ahmad, M.; Manzoor, K.; Venkatachalam, P.; Ikram, S.; *Int. J. Biol. Macromol.*, **2016**, *92*, 910. DOI: https://doi.org/10.1016/j.ijbiomac.2016.07.075.
31. Ghosal, P. S.; Gupta, A. K.; *RSC Adv.*, **2015**, *5*, 105889.
32. Kumar, P. S.; Ramalingam, S.; Kirupha, S. D.; Murugesan, A.; Vidhyadevi, T.; Sivanesan, S.; *Chem. Eng. J.*, **2011**, *167*, 122.
33. Ayawei, N.; Ebelegi, A. N.; Wankasi, D.; *J. Chem.*, **2017**, *2017*.
34. Eljamal, O.; *et al.*, *J. Water Process Eng.*, **2022**, *46*, 102608. DOI: https://doi.org/10.1016/j.jwpe.2022.102608.
35. Maamoun, I.; *et al.*, *J. Mol. Liq.*, **2022**, *358*, 119216. DOI: https://doi.org/10.1016/j.molliq.2022.119216.
36. Eljamal, O.; *et al.*, *Chemosphere*, **2022**, *287*, 131990. DOI: https://doi.org/10.1016/j.chemosphere.2021.131990.
37. Taguba, M. A. M.; *et al.*, *Water*, **2021**, *13*, 1662.
38. Hanna, A. A.; Abdelmoaty, A. S.; Sherief, M. A.; *J. Chem.*, **2019**, *2019*. DOI: 10.1155/2019/1805280.
39. Kanel, S. R.; Manning, B.; Charlet, L.; Choi, H.; *Environ. Sci. Technol.*, **2005**, *39*, 1291. DOI: 10.1021/es048991u.
40. Ezeabasili, A. C. C.; Anike, O. L.; Okoro, B. U.; U-Dominic, C. M.; *African J. Environ. Sci. Technol.*, **2014**, *8*, 491.
41. Palmer, M. J.; *et al.*, *Sci. Total Environ.*, **2021**, *776*, 145926.
42. Eljamal, R.; Eljamal, O.; Khalil, A. M. E.; Saha, B. B.; Matsunaga, N.; *J. Environ. Chem. Eng.*, **2018**, *6*, 4727. DOI: 10.1016/j.jece.2018.06.069.
43. Manning, B.; *Microchim. Acta*, **2005**, *151*, 181.
44. Mercer, K.L.; Tobiason, J.E.; *Environ. Sci. Technol.*, **2008**, *42*, 3797.
45. Wallace, S. H.; Shaw, S.; Morris, K.; Small, J. S.; Fuller, A. J.; Burke, I. T.; *Appl. Geochemistry*, **2012**, *27*, 1482. DOI: https://doi.org/10.1016/j.apgeochem.2012.04.007.
46. Prot, T.; Korving, L.; Van Loosdrecht, M. C. M.; *Water Sci. Technol.*, **2022**, *85*, 1920. DOI: 10.2166/wst.2022.057.
47. Liu, A.; Liu, J.; Zhang, W.; *Chemosphere*, **2015**, *119*, 1068. DOI: https://doi.org/10.1016/j.chemosphere.2014.09.026.
48. Liu, H.; *et al.*, *Chem. Eng. J.*, **2013**, *234*, 80.

49. Li, S.; Wang, W.; Liang, F.; Zhang, W.; *J. Hazard. Mater.*, **2017**, *322,* 163. DOI: https://doi.org/10.1016/j.jhazmat.2016.01.032.
50. Ramos, M.A.V.; Yan, W.; Li, X.; Koel, B. E.; Zhang, W.; *J. Phys. Chem. C*, **2009**, *113,* 14591. DOI: 10.1021/jp9051837.
51. Yan, W.; Vasic, R.; Frenkel, A. I.; Koel, B. E.; *Environ. Sci. Technol.*, **2012**, *46,* 7018. DOI: 10.1021/es2039695.
52. Mauricio, A.V.; *Chem. Commun.*, **2010**, *46,* 6995.

AUTHORS BIOGRAPHY

Ibrahim Maamoun obtained his M.Sc. (2018) and Ph.D. (2021) in energy and environmental engineering from the Interdisciplinary Graduate School of Engineering Sciences (IGSES), Kyushu University, Fukuoka, Japan. Currently, he works as a post-doctoral researcher at the Advanced Science Research Center (ASCR), Japan Atomic Energy Agency (JAEA), Ibaraki, Japan. His main research interests are water treatment (i.e., removal of different contaminants from contaminated surface water, groundwater, and wastewater), environmental nanotechnology, solid/liquid interactions, and radiochemistry.

GRAPHICAL ABSTRACT

Arsenic removal by magnesium hydroxide coated iron nanoparticles ($nFe^0@Mg(OH)_2$)